International Journal of Coal Science & Technology (2023) 10:15
https://doi.org/10.1007/s40789-023-00571-y

RESEARCH

Theoretical and numerical simulation investigation of deep hole dispersed charge cut blasting

Chengxiao Li[1] · Renshu Yang[1,2] · Yanbing Wang[1] · Yiqiang Kang[1] · Yuantong Zhang[1] · Pin Xie[3]

Received: 14 June 2022 / Revised: 10 November 2022 / Accepted: 16 January 2023

Abstract
Drilling and blasting methods have been used as a common driving technique for shallow-hole driving and blasting in rock roadways. With the advent of digital electronic detonators and the need for increased production efficiency, the traditional blasting design is no longer suitable for deep hole blasting. In this paper, a disperse charge cut blasting method was proposed to address the issues of low excavation depth and high block rate in deep hole undercut blasting. First, a blasting model was used to illustrate the mechanism of the deep hole dispersive charge cut blasting process. Then, continuous charge and dispersed charge blasting models were developed using the smooth particle hydrodynamics-finite element method (SPH-FEM). The cutting parameters were determined theoretically, and the cutting efficiency was introduced to evaluate the cutting effect. The blasting effects of the two charging models were analyzed utilizing the evolution law of rock damage, the number of rock particles thrown, and the cutting efficiency. The results show that using a dispersed charge improves the cutting efficiency by about 20% and the rock breakage for the deep hole cut blasting compared to the traditional continuous charge. In addition, important parameters such as cutting hole spacing, cutting hole depth and upper charge proportion also have a significant impact on the cutting effect. Finally, the deep hole dispersed charge cut blasting technology is combined with the digital electronic detonator through the field engineering practice. It provides a reference for the subsequent deep hole cutting blasting and the use of electronic detonators in rock roadways.

Keywords Deep hole blasting · Cut blasting · Dispersed charge · SPH-FEM · Digital electronic detonator

1 Introduction

Drilling and blasting methods are essential for rock excavation and have been extensively used in tunnels, shafts, roadways and open-pit mining (Xie et al. 2016a, b; Liu et al. 2018; Li et al. 2021, 2022). As the initial step of blasting excavation in the process of roadway blasting and excavation, cut blasting impacts the excavation efficiency. The current application of cut blasting in shallow holes has achieved good results, but it is still not widely used in deep holes due to instrumental and technical reasons. With the continued improvement of safety and efficiency requirements in mining production, reducing the number of operations and improving the efficiency of single excavation will become the main goals of rock excavation in the future. Therefore, studying the application of cut blasting in deep holes is significant.

The current cutting methods are primarily divided into oblique holes and parallel cutting (Amiri and Murthy 2019; Adhikari et al. 1999; Xie et al. 2016a, b; Zuo et al. 2018; Liu et al. 2019; Tang et al. 2022). The advantage of oblique hole cutting is that the cavity formed after blasting is large, while the disadvantage is that the drilling accuracy is high, and the section size limits the hole spacing as the hole depth increases. Consequently, oblique hole undercut is mainly implemented in shallow hole undercut (Yang et al. 2020). The advantage of parallel hole cutting is that the drilling is simple and the hole depth can be increased arbitrarily. The disadvantage is that the size of the cavity created by a single hole does not increase unlimitedly with the charge's length and the resistance line also rises (Henrych 1979; Li et al.

✉ Chengxiao Li
licx93@163.com

1 School of Mechanics and Civil Engineering, China University of Mining and Technology-Beijing, Beijing 100083, China

2 School of Civil and Resource Engineering, University of Science and Technology Beijing, Beijing 100083, China

3 Gubei Coal Mine of Huaizhe Coal and Electricity Co., Ltd, Huainan 232150, China

Published online: 11 March 2023

2020). This reduces the effectiveness of the cut blasting, so multi-stage cut blasting is employed to enhance the blasting effect in shaft cut blasting. However, according to China's safety blasting regulations, the blasting interval in mine roadways cannot exceed 130 ms, and the commonly used detonators have only 5 intervals. Hence, it is impossible to implement multi-level parallel hole cutting blasting on roadways at this time. It is necessary to propose a cut blasting technology suitable for deep hole excavation in the roadway to improve the cutting efficiency, given the problems associated with using cutting technology in roadway excavation.

Many scholars have examined the relationship between cutting form and cutting efficiency. Shapiro compared parallel and large-diameter hole cutting, and established a new evaluation index to quantify the difference in effect caused by various cutting forms (Shapiro 1989). Soroush et al. established a blasting design software for tunnel cutting, and utilized it to compare the impact of parallel and oblique hole cutting (Soroush et al. 2015). Cheng et al. simulated the blasting effect of parallel hole cutting with the charge at the bottom of the hole (Cheng et al. 2021). The research revealed that the new cutting method increases the average excavation depth and reduces the unit consumption compared to the form without charge at the bottom of the hole. Zhang et al. investigated the influence of large-diameter holes on the blasting effect of parallel hole cutting, and analyzed the effect of blast stress waves and blasting gas (Zhang et al. 2020). They also obtained blasting parameters such as cutting hole spacing and diameter through theoretical calculations and applied the results to engineering practice. Yue et al. examined the impact of voids on blast stress waves (Yue et al. 2009). The test indicated that voids significantly influence the transmission of stress waves. Near the voids, the stress wave generates the largest principal stress difference, and the maximum tensile stress is perpendicular to the direction of the stress wave. The direction of the connection line of the blasthole has changed considerably. Zhang et al. applied SPH-FEM to analyze the effect of charge at the bottom of the hole on the blasting effect of undercut and various cutting parameters on the blasting effect through the rock throwing process and cutting efficiency (Zhang et al. 2022).

In addition to the cutting form, other cutting parameters also have an important impact on the blasting effect. Himanshu et al. analyzed the quantitative relationship between holes and blastholes (Himanshu et al. 2021). The study showed that the ratio of the number of holes to blastholes has a greater impact on the deformation mode of the rock mass than the number of holes themselves. The number of gun holes can be reduced by optimizing the relationship between the two types of holes. Ding et al. investigated the influence of charge proportion on vertical shaft blasting effect (Ding et al. 2021). The findings showed that when the upper charge ratio was 0.42, the fractal dimension of the cavity generated by the explosion was the largest. Qiu et al. analyzed the impact of time-delayed blasting on the blasting effect in the case of a single free surface. They discovered that the rock-breaking effect of the interaction between the stress wave and the blasting gas caused by the delayed blasting is superior to the superposition effect of the stress wave caused by the simultaneous blasting (Qiu et al. 2018). The superposition of stress waves does not promote the formation of a blasting cater. Gong et al. examined the influence of the presence or absence of cut holes on the effect of undercut blasting (Gong et al. 2015). The results of field practice and numerical simulation showed that blasting at the center hole increases the stress peak in the undercut area and rises the section's fractured area. Liu determined the delay time of electronic detonator in tunnel blasting and the amount of charge in the cutting hole by analyzing the vibration curve, and studied the conditions of different free surfaces (Liu et al. 2021).

For the coal mine drift blasting, although the previous research has made a lot of adjustments to the cutting form and parameters, the final effect is still in the shallow hole blasting. The cutting blasting efficiency in coal mine drifts has not made major breakthroughs in the past decades. The rise of digital electronic detonators has made it possible to make a breakthrough in the cut blasting technology of coal mine drift. Therefore, this paper proposes a deep hole dispersed charge blasting technology for underground mine roadway blasting, which addresses the issue of low deep hole blasting efficiency and difficult rock throwing. Firstly, a parallel hole undercut blasting model is established, and the blasting mechanism of the deep hole segmented charge is analyzed theoretically. Then, the blasting process of the modern and the traditional blasting technology is simulated, and the influence of different cutting parameters is analyzed. Finally, the deep hole segmented charge blasting technology was successfully implemented in the roadway excavation and blasting project of the Huainan Gubei Mine with the aid of an electronic detonator. It provides a reference for the combination of deep hole cutting blasting and electronic detonator in the roadway in the future.

2 Deep hole dispersed cut blasting model and its mechanism analysis

2.1 Deep hole dispersed cut blasting technology

As mentioned previously, this paper proposes a deep hole dispersed charge cut blasting technology to improve the excavation efficiency of deep hole cut blasting. This technology's core is represented by changing the traditional continuous charge to the dispersed charge. Figure 1 shows the layout of the cutting holes. It can be seen that parallel

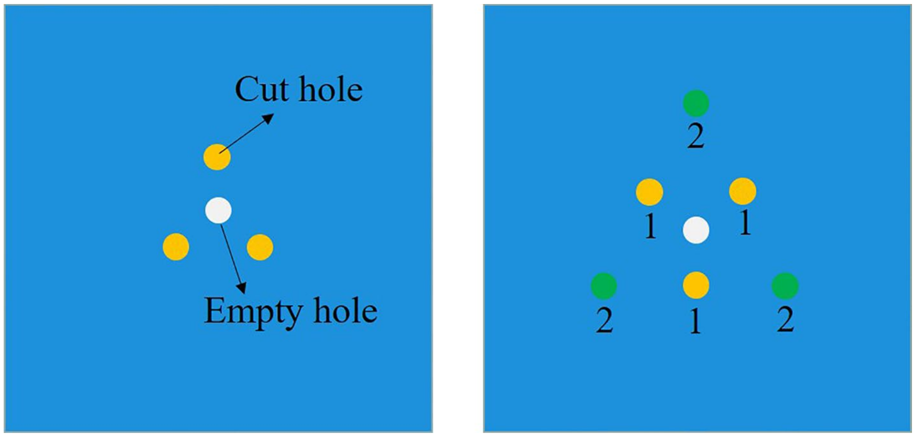

(a) Layout of triangular parallel cut holes (b) Layout of double triangular parallel cut holes

Fig. 1 Layout of cut holes. **a** Layout of triangular parallel cut holes **b** Layout of double triangular parallel cut holes

holes are more suitable for deep hole cutting blasting than inclined holes. Indeed, the triangular arrangement drilling method has the advantages of fewer holes and higher cutting efficiency (Dai and Yang 2000). Therefore, this technique is adopted in this paper. In Fig. 1a, an empty hole is arranged at the center of the three cut holes to provide compensation space and a guiding effect, so that the rock in the cut area can be broken more evenly after blasting. With the increase of cross-sectional area or rock hardness, using three cut holes only cannot meet the purpose and effect of cut blasting. As a result, adding a circle of cut holes is necessary based on the actual situation, as shown in Fig. 1b. The three cutting holes closest to the central hole are named the first order cut hole, detonated first, and the three outermost holes are named the second order cut hole. The hole is detonated after the first order cut hole. The first blasting hole is the hardest to break through since. It only has a single free surface, and is the strongest clamped by the rock. It also creates a compensation space for subsequent blasting. Therefore, this study focuses on blasting the first-order cut hole, and conducting relevant simulation research.

As mentioned above, the importance of blasting the first-order cut blasting, the dispersed charging technology is adopted for the charge of the first-order cut blasting. Figure 2 shows two forms of charging. The dispersive charge uses the mud to change the explosive from the original adjacent placement into several parts. For the 2.5–3.0 m cut hole, it is more appropriate to divide the explosive into two sections.

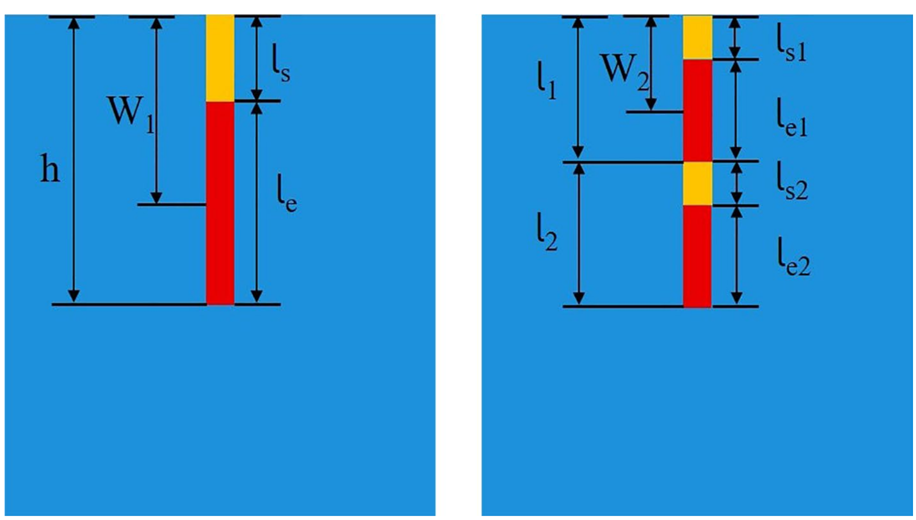

(a) Continuous charge (b) Distributed Charge

Fig. 2 Charge structure comparison. **a** Continuous charge **b** Distributed charge

In the blasting and excavation of the rock roadway of the coal mine in the past, due to the limitation of the delay time of the detonator allowed in the coal mine (there are only five delay times) and the limitation of the length of the drill pipe, the blasthole depth is usually about 2.0 m. The delay time is typically set between the blastholes, whereas there is no extra delay time used in the blasthole. Thus, there is no possibility of dispersive charge blasting. With the rise of electronic detonators, the blasting of rock tunnels in coal mines can achieve dispersed charge blasting. For the two charging methods in Fig. 2, their blocking lengths are the same ($l_s = l_{s1} + l_{s2}$) and their explosives have the same length ($l_e = l_{e1} + l_{e2}$). It can be seen from the figure that the minimum resistance line W_1 of the continuous charge is much larger than that of the dispersed charge. When the drilling depth increases, the size of the resistance line will seriously affect the formation and blasting effect of the blasting funnel (Wang et al. 2013; Saadatmand and Katsabanis 2020). In the dispersed charge structure, the charge near the free surface l_1 is called the upper charge, and that near the bottom of the drilled hole l_2 is called the lower charge. The lengths of l_1 and l_2 are sensitive parameters that affect the cutting effect. The ratio of the upper charge bag to the drilling depth is called the upper charge ratio (η), that is, $\eta = l_1/(l_1 + l_2)$.

2.2 Process and mechanism analysis of dispersed charge cut blasting

The rock-breaking process of the columnar charge can be simplified into two stages. The first stage is the blast stress wave's direct damage to the rock. In this stage, the rock mass close to the free surface forms a cavity under the action of the blast stress wave and reflected tensile wave, and the remaining rock mass is pushed to the free surface under the action of the blast gas (Lin and Chen 2005; Zhang et al. 2000; Li et al. 2019). Figure 3 shows the blasting process of deep hole dispersive charge cutting, and Fig. 3a shows the state when the rock mass has not yet been detonated. It can be seen that when the upper charge is detonated, due to the small minimum resistance line, the rock can be quickly broken and thrown to the free surface and form a cavity, which creates a new free surface for the lower rock mass that has not been detonated (Fig. 3b). The lower rock mass reduces its minimum resistance line in the presence of the new free surface, which means that the lower rock mass can be thrown out of the cavity smoothly. Figure 3c shows the cavity formed after the first-order undercut hole is completely blasted. Since the first-order undercuts use dispersive charge, the effect of forming a cavity within the first-order undercuts is good, and the compensation space provided is sufficient for the detonation of the second-order undercuts and other blasting holes.

In order to better understand the blasting process of dispersed charge, the following assumptions are made to simplify the blasting process:

(1) The clay is compressed into a very small segment at the moment of explosion, and the gas–solid mixture formed by the crushed stone and the explosive gas formed during the cutting blasting process are considered to be fluid.
(2) Since the drilling hole through the rock roadway excavation blasting is horizontal, gravity will not affect the horizontally thrown gravel in the cavity. Thus, it is considered that the only resistance of gravel in the throwing process is the friction with the cavity wall.
(3) The gas–solid mixture moves in one dimension along the horizontal direction.

2.3 Blasting parameter calculation

2.3.1 Calculation of cutting hole spacing

The choice of the spacing between the cutting holes directly affects the cutting efficiency. When the spacing

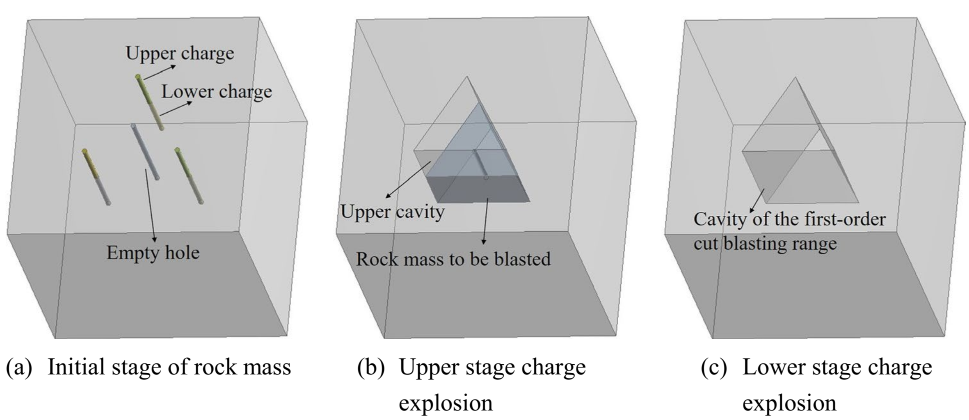

Fig. 3 Dispersed charge blasting process. **a** Initial stage of rock mass **b** Upper stage charge explosion **c** Lower stage charge explosion

is too large, it is easy to obtain large pieces of gravel, and when the spacing is too small, the explosive's energy is wasted. Therefore, the spacing of the cutting holes should be determined according to the rock and the explosive properties. The blasting gas produced by the explosion of the explosive quickly fills the blasthole, and the initial pressure acting on the blasthole wall is defined as follows (Henrych 1979):

$$P_0 = \frac{1}{2(\gamma + 1)}\rho_0 D_0^2 \tag{1}$$

where ρ_0 is explosive density, D_0 is explosive detonation speed, γ is the adiabatic entropy exponent of the explosion process, usually taken as 3.

The explosive gas that expands is considered to be an ideal gas, its expansion process is assumed to be isentropic adiabatic, and its expression is (Zong 1997):

$$P_0 V_0^\gamma = \text{Const} \tag{2}$$

where V_0 is the inverse of the density of the explosive.

$$P_0 V_0^\gamma = P_x V_x^\gamma \tag{3}$$

$$P_x = P_0\left(\frac{V_0}{V_x}\right)^\gamma \tag{4}$$

$$V_0 = \frac{1}{\rho_0} = \frac{V_0'}{m_0} \tag{5}$$

where V_0' is the initial volume of the explosive gas.

$$V_0' = \pi r_b^2 l_e \tag{6}$$

$$V_x' = (\pi r_b^2 + n r_c a) l_e + \pi r_b^2 x \tag{7}$$

where r_b is the radius of the blast hole, r_c is the crack width, n is the number of cracks in a single blast hole, usually taken as 8, and x is the displacement of the compressed clay.

For a rock to crack, the pressure must be greater than the tensile strength. This phenomenon is represented mathematically as follows:

$$P_x \geq \sigma_{td} \tag{8}$$

Combining Eqs. (4), (7) and (8) to get the following equation:

$$a \leq \frac{1}{4na}\left\{\pi r_b^2\left[\left(\frac{P_0}{\sigma_{td}}\right)^{\frac{1}{\gamma}} - 1\right] - \frac{\pi r_b^2 x}{l_e}\right\} \tag{9}$$

where, the value of a determines the cut hole spacing L.

2.3.2 Delay time interval

The main advantage of the deep hole dispersive charge cut blasting technology is that the upper charge is firstly detonated, and the lower charge is detonated after a delay. The upper detonation provides a free surface for the lower rock to be thrown. Therefore, a reasonable delay determines whether the upper charge can form a sufficient cavity. The excavation and blasting construction of the coal mine rock roadway is limited by the total delay time of 130 ms. This means that the time interval between the upper and lower charges is limited. Thus, the delay time should at least satisfy the time required for the explosive to complete the detonation transfer in the blasthole and the formation of the fracture zone. The time taken by the explosive to detonate is:

$$t_1 = \frac{l_{e1}}{D_0} \tag{10}$$

The formation time of the fissure area caused by the explosion is (Lu et al. 2012):

$$t_2 = \frac{\sqrt{1/4L^2 + l_{s1}^2}}{C_f} \tag{11}$$

where C_f is the average velocity of rock crack propagation, usually taken as 0.2–0.3 of the C_p, and C_p is the rock longitudinal wave velocity.

The interval between the detonation of the upper charge and the lower charge is defined as follows:

$$t \geq t_1 + t_2 \tag{12}$$

2.3.3 Calculation of cutting efficiency

Coal mine drift excavation has the characteristics of a single free face, which makes the crushed stone thrown in the direction of the free face. The cutting area accounts for a

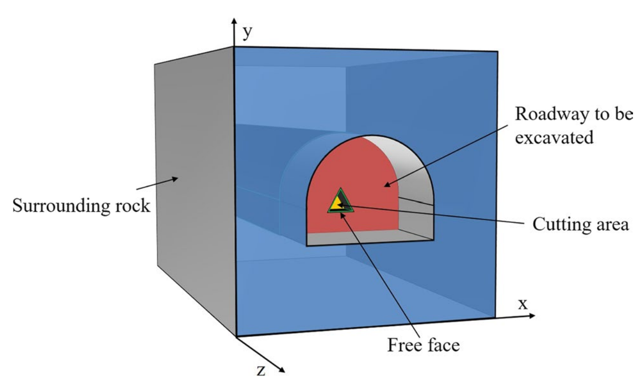

Fig. 4 Schematic diagram of cut blasting in coal mine roadway

small section area, so the free surface has a greater constraint on cutting blasting. This causes the crushed stone in the cutting area to move almost along the direction of the free surface. As the first blasting hole, the direction of the minimum resistance line of the cutting hole is unique (as shown in Fig. 4).

Based on the assumptions proposed in Sect. 2.2, it is assumed that the movement of the gravel and the explosive gas in the cavity conforms to the one-dimensional unsteady fluid law (Lin and Chen 1997; Zhang et al. 2021), and the basic equation is:

$$\begin{cases} \dfrac{\partial \rho'}{\partial t} + \dfrac{\partial}{\partial t}(\rho \upsilon) = 0 \\ \dfrac{\partial \upsilon}{\partial t} + \upsilon \dfrac{\partial \upsilon}{\partial x} - \dfrac{1}{\rho}\dfrac{\partial P'}{\partial x} = 0 \\ \dfrac{\partial}{\partial t}\left(\dfrac{P'}{\rho'^{\gamma}} + \upsilon \dfrac{\partial}{\partial x}\left(\dfrac{P'}{\rho'^{\gamma}}\right)\right) = 0 \end{cases} \tag{13}$$

where ρ' and P' refer to the density and pressure of the gas–solid mixture, respectively, and υ is the expansion rate of the mixture.

The initial conditions of the equation are:

$$\begin{cases} \upsilon = 0 \\ P_1 = \dfrac{3r_b^2}{r_0^2 + 3r_b^2} P_0 \end{cases} \tag{14}$$

where r_0 is the hole radius.

Assuming that the explosive gas provides the power of the crushed stone in the cavity, and the resistance comes from the frictional force with the cavity wall, the following expressions can be defined:

$$F_g = \frac{\sqrt{3}}{4} P_1 L^2 \tag{15}$$

$$I_f = 3P_1 L(h - h_d)\frac{\mu}{1-\mu} fT \tag{16}$$

where T is the action time of the explosive gas, which depends on the expansion time of the explosive gas and can be expressed as $T = \frac{h}{C_0(8^{\frac{1}{\gamma}} - 1)}$, C_0 is the sound velocity of the mixture product, and μ is the poisson's ratio of the mixture, which is taken as 0.6.

Based on the impulse theorem, combined with Eqs. (15) and (16), the initial velocity of the gas–solid mixture can be obtained as follows:

$$I_g - I_f = M\upsilon_0 \tag{17}$$

$$\upsilon_0 = \frac{1}{M}\left(\frac{\sqrt{3}}{4} P_1 L^2 T - 3P_1 L(h - h_d)\frac{\mu}{1-\mu} fT\right) \tag{18}$$

where M is the mass of the gas–solid mixture.

The gas–solid mixture moves to the free surface under the action of overcoming the friction force. When it moves to the x position, the resultant force on the gas–solid mixture is as follows:

$$F_x = F_g \frac{h - h_d}{h - h_d + x} - F_f(h - h_d - x) \tag{19}$$

The equations of motion can be obtained from Newton's laws:

$$a = \frac{d^2 x}{dt^2} = \frac{F_x}{M} \tag{20}$$

further there are:

$$\frac{d^2 x}{dt^2} = \frac{P_1}{\rho'}\left(\frac{h - h_d}{(h - h_d + x)(h - h_d - x)} - \frac{4\sqrt{3}\eta}{1-\eta}\frac{f}{L}\right) \tag{21}$$

By applying the boundary conditions ($x = 0$, $\upsilon_x = \upsilon_0$) to the above formula, the following equation can be derived:

$$\frac{P_1}{\rho'}\left(\frac{1}{2}\ln\frac{(h - h_d + x)}{(h - h_d - x)} - \frac{4\sqrt{3}\eta}{1-\eta}\frac{f}{L}x\right) + \upsilon_0^2 = 0 \tag{22}$$

The depth of the blasting funnel produced by the explosion is based on (Zhang et al. 2000):

$$h_d = \left[1 + 0.36\sqrt{\gamma}\frac{D_0}{C_p}\right] l_s \tag{23}$$

According to Eq. (22), the moving distance $x_{\upsilon=0}$ of the gas–solid mixture can be obtained when the moving speed is 0, and then the cutting efficiency can be defined as:

$$E_c = \frac{h_d + x_{\upsilon=0}}{h} \tag{24}$$

The upper charge is detonated first to form a cavity for the dispersed charge structure. Although some gravel may still be left in the cavity, the lower charge can push the remaining partial gravel out of the free surface. It can be considered that when the proportion of the upper charge is at an appropriate value, the rock in the upper charge range can be completely thrown out of the free surface, and the cutting efficiency at this time is defined as follows:

$$E_n = \frac{l_1 + h'_d + x'_{x=0}}{h} \tag{25}$$

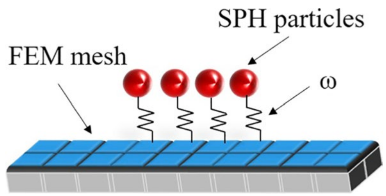

Fig. 5 SPH particles coupled with FEM elements

Among them, h'_{d} and $x'_{x=0}$ are the depth of the blasting funnel formed after the lower charge is detonated and the moving distance of the gas–solid mixture, respectively.

3 Smoothed particle hydrodynamics-finite element method (SPH-FEM) for the cut blasting

3.1 Simulation method selection and principle

The existing simulation methods include finite element, discrete element, continuous and discontinuous method, etc. They have their own emphasis on different research contents. In the process of undercut blasting, severe deformation and rock fragmentation occur near the blasthole. At the same time, the rock mass cannot be set to a large size due to the calculation time, so it is necessary to consider a stable solution when the rock mass boundary is stressed. Since the smooth particle hydrodynamics has no mesh, its self-adaptability can handle the large deformation and large displacement of the material well in the calculation. However, the SPH method is computationally inefficient and unsuitable for boundary processing (Jayasinghe et al. 2019). Therefore, the idea of combining SPH and FEM methods is to use SPH to deal with the rocks near the blast hole, and utilize FEM to deal with the force of the far boundary rocks.

Indeed, an appropriate definition of how the SPH contacts the FEM is key to the simulation process. To prevent the calculation instability due to grid distortion caused by abnormal SPH particles passing through the FEM grid, a penalty contact is added between the grid and the particles (as shown in Fig. 5). It can be used to determine whether particles will pass through the mesh. When particles have the potential to pass through the mesh, a spring-like contact force is applied between the two. The magnitude of this force is related to the depth of the particles entering the mesh, and this contact force is used to prevent damage to the mesh caused by abnormal particles. The contact force (ω) can be expressed as:

$$\omega = \max\left(\eta_1 \frac{KS_{\mathrm{g}}^2}{V},\quad \eta_2 \frac{m_{\mathrm{n}}}{\Delta t^2}\right) \tag{26}$$

3.2 Verification of the SPH-FEM approach

Before using SPH-FEM method to simulate the rock blasting process, rigorous prove is required, and the verification focuses on the following parts:

(1) Conduct convergence analysis to verify particle size.
(2) Verify whether the explosion stress wave can be continuously transmitted from the SPH particles to the FEM mesh.
(3) Verify the ability to simulate rock blasting.

To complete the above verification process, a plane blasting model is established, as shown in Fig. 6. The outermost layer of the model is composed of 5 m × 5 m FEM grid, and the middle region is composed of 3 m × 3 m SPH particles. A blast hole with a radius of 5 cm is set in the center of the model, and the explosive is fully coupled with the blast hole. The SPH particles are converted from the FEM mesh, and the particle size is 5 cm × 5 cm. In addition, a model with particle size of 3 cm × 3 cm is also established. The contact of CONTACT_TIED_ NODES_ TO_SURFACE is set between FEM and SPH. Two measuring points G_{a} and G_{b} are respectively set at the contact surface, where G_{a} is used to detect the pressure change at the SPH particle and G_{b} is used to detect the pressure change at the FEM unit.

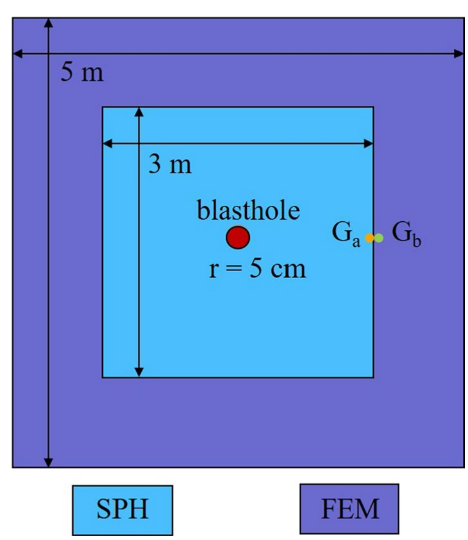

Fig. 6 Plane model for SPH-FEM approach

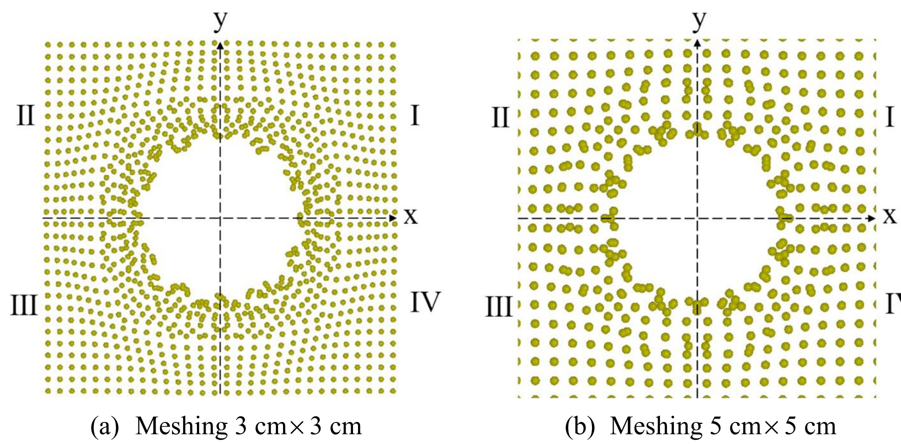

Fig. 7 Particle motion with different mesh size. **a** Meshing 3 cm × 3 cm **b** Meshing 5 cm × 5 cm

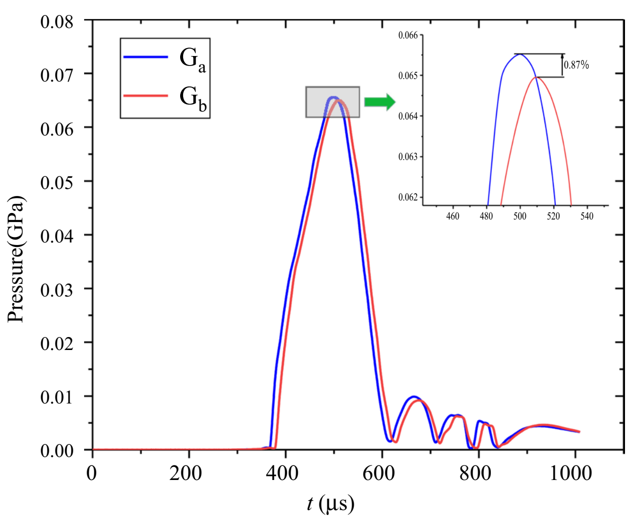

Fig. 8 Pressure change of measuring point at interface

The selection of rock and explosive materials is described in Sect. 3.3.2.

There is no grid connection between SPH particles, and particles can move freely. Therefore, the movement trend and trajectory of particles have an important impact on the simulation results. Figure 7 shows the movement trend of SPH particles after explosion under two sizes. Because the model is large, some areas near the blast hole are selected for magnification. Through visual comparison, it can be found that the movement trend of particles under the two sizes is basically the same, both of which are uniformly diffused from the blast hole to the surrounding. The particle distribution is divided into four quadrants based on the center of the blast hole. According to statistics, the number of particles in the four quadrants in Fig. 7a is the same, and the number of particles in the four quadrants in Fig. 7b is also the same. This shows that the particle size change will not significantly change

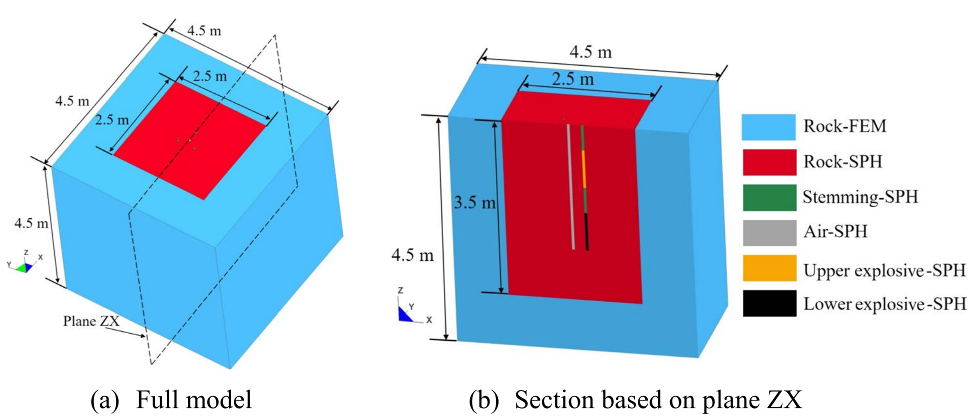

Fig. 9 Deep hole cutting and blasting model. **a** Full model **b** Section based on plane *ZX*

the direction of motion of the particle, but will increase the number of particles in the unit area. Therefore, the particle size with a side length of 5 cm is reasonable. Figure 8 shows the pressure change of two measuring points on the contact surface. It shows that the pressure peak value of measuring point G_a is higher than that of measuring point G_b. The pressure peaks of the two measuring points are almost the same, which proves that the stress can be transferred smoothly from the particle area to the grid area. The above simulation results have been successfully verified.

3.3 Models and materials

3.3.1 Model parameters

Figure 9 shows the SPH-FEM coupling technology's deep hole cutting blasting model. In order to ensure the stability of the calculation, a full model is established (Fig. 9a), and the outer layer of the model is wrapped by the FEM mesh. A cube with dimensions of 4.5 m × 4.5 m × 4.5 m, with non-reflective boundaries imposed on the four sides and bottom of the FEM region. The middle is composed of SPH particles, and the size is a cuboid of 2.5 m × 2.5 m × 3.5 m. The grid size is 5 cm, and the part of the blast hole is locally refined. The number of FEM elements is 554,000 and the number of SPH particles is 223,550. The cross-sectional view of Fig. 9b is obtained by taking a cut along the plane *ZX* where the line connecting one of the cut holes and the empty holes is located. It can be seen that the charge in the cut hole adopts a dispersed charge, and the empty hole is filled with air.

The selection of various cutting parameters in the model comes from previous field practice cases. The holes' depth and diameter are 2.5 m and 42 mm respectively. The total explosive length of the cut hole is 1.75 m, and the stemming length is 0.75 m. The proportion of charge in the upper section is $\eta = 0.5$. Hence, $l_{s1} = l_{s2} = 0.375$ m and $l_{e1} = l_{e2} = 0.875$ m. Based on Eq. (9), a is calculated as 458 mm, and the spacing L of the cutting holes in the simulation is 450 mm. The interval between the detonation of the upper explosive and the lower explosive is 10 ms, which is greater than the delay time calculated by Eq. (12). Thus, the detonation of the upper explosive is sufficient to create a new free surface.

3.3.2 Material

Since the simulation is the process of rock cutting and blasting, the selected rock material is required to reflect the damage evolution. The Holmquist-Johnson–Cook (HJC) constitutive model is widely used to simulate the rock under large deformations, high strain rates and high temperatures and pressures (Johnson and Holmquist 2011). The constitutive model mainly consist of a state equation, a strength equation and a damage model. The damage consists of plastic strain and plastic volume strain, which can be expressed as:

$$D = \sum \frac{d\varepsilon_p + d\mu_p}{D_1 (P^* + T^*)^{D_2}} \tag{27}$$

where ε_p and μ_p are the equivalent plastic strain and plastic volume strain, respectively, P^* is the normalized hydrostatic pressure, T^* is the normalized tensile hydrostatic pressure, and D_1 and D_2 are damage constants.

In this paper, the basic parameters of rock are measured by Li (2016), and the parameters required by HJC are calculated by Wang et al. (2021). The main parameters of the rocks are given in Table 1.

Table 1 Parameters values for HJC

Density (kg/m^3)	Compressive strength (MPa)	Normalized cohesive strength	Shear modulus (GPa)	Damage constant D_1	Damage constant D_2
2700	119	0.866	24.17	0.04	1

The explosive uses the JWL state equation (Alia and Souli 2006):

$$P = A\left(1 - \frac{\omega}{R_1 V}\right)e^{-R_1 V} + B\left(1 - \frac{\omega}{R_2 V}\right)e^{-R_2 V} + \frac{\omega E}{V} \tag{28}$$

To make the work ability of the explosive in the simulation approximate to the field practice, the explosives selected in simulation are the three-level water gel explosives. The density of the explosive is 1150 kg/m^3, the detonation velocity of the explosive is 3200 m/s, and the relevant parameters of the state equation are given in Table 2 (Wang et al. 2017).

Table 2 Parameters values for explosive

A (GPa)	B (GPa)	ω	R_1	R_2	E (GPa)
420	0.45	0.36	3.55	0.16	3.15

The stemming material is soil, which is similar to the tap mud used in field practice, and its parameters are given in the reference (Zhang et al. 2022). Besides, the air is considered to conform to the ideal gas law, and the parameters are given in the reference (Esmaeili and Tavakoli 2019).

3.4 Simulation results

Figure 10 shows the damage evolution process of deep hole dispersed charge cut blasting. Section ABCD is taken at a

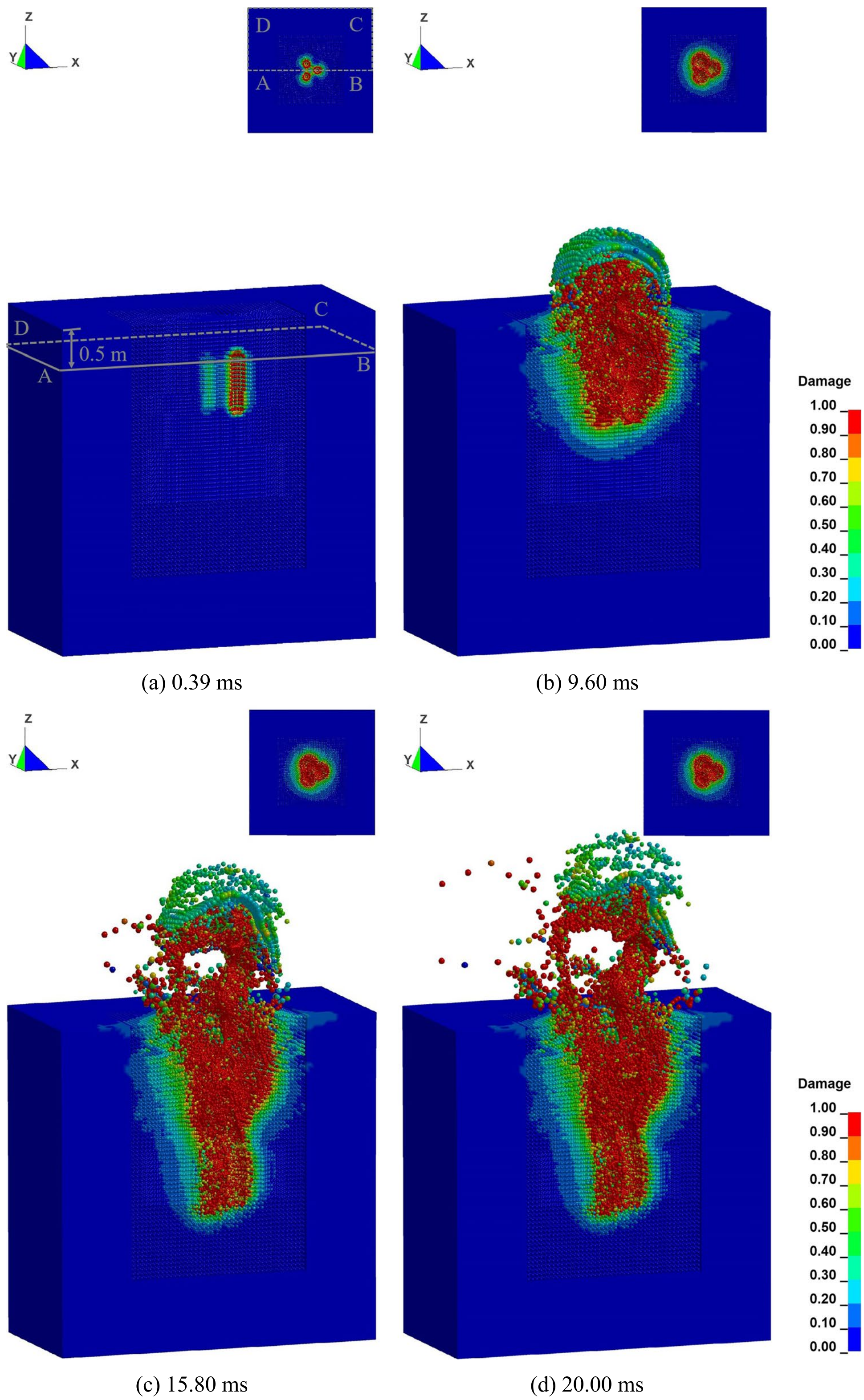

Fig. 10 Deep hole dispersed charge cut blasting process. **a** 0.39 ms; **b** 9.60 ms; **c** 15.80 ms; **d** 20.00 ms

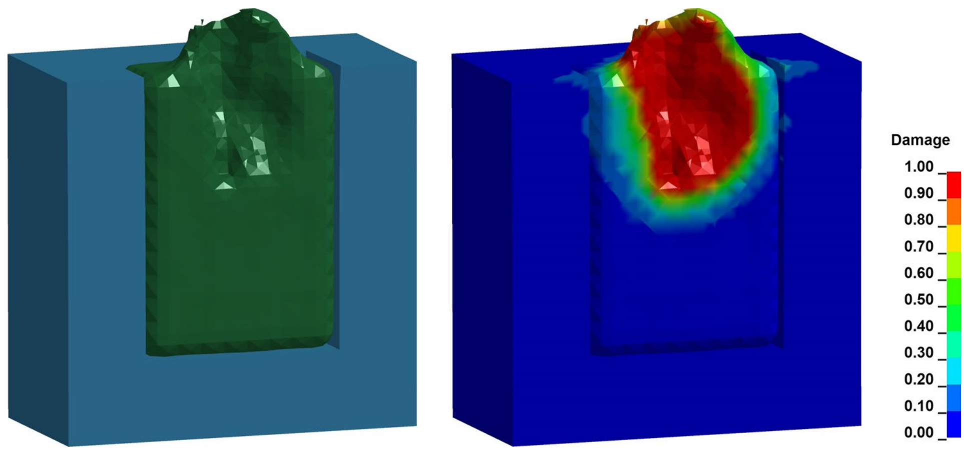

(a) Surface diagram of the cavity formed by the upper charge (b) Damage evolution of surfaces

Fig. 11 Cavity surface map of deep hole dispersed charge cut blasting at 8.39 ms. **a** Surface diagram of the cavity formed by the upper charge; **b** Damage evolution of surfaces

distance of 0.5 m from the free surface, and the upper right corner of each picture is the damage evolution near the blasthole of this section. When t was 9.60 ms, the rock near the upper charge was thrown out of the free surface, and with the detonation of the lower charge, the rock in the range of the cut hole was further thrown out of the free surface. Figure 11 shows the surface graph of the cavity formed by cut blasting at $t = 8.39$ ms. At this time, the lower part of the charge has not yet detonated, and the upper part of the charge has formed a larger cavity after detonation. This provides compensation space and a new free surface for the lower charge cut blasting, which is consistent with the deep hole dispersion cut blasting process shown in Fig. 3.

Figure 12 shows the continuous charge cut blasting process. All the explosives in Fig. 12a are detonated at one time due to the continuous charge used in the cut. Since the explosives are concentrated at the bottom of the blasthole, it is difficult for the rock to be thrown out of the free face quickly. Figure 12b shows that some rocks are thrown out of the free surface, but the uppermost part of the rock is in a state of undamaged and slightly damaged. Compared with the scattered cut blasting process in Fig. 12, the continuous

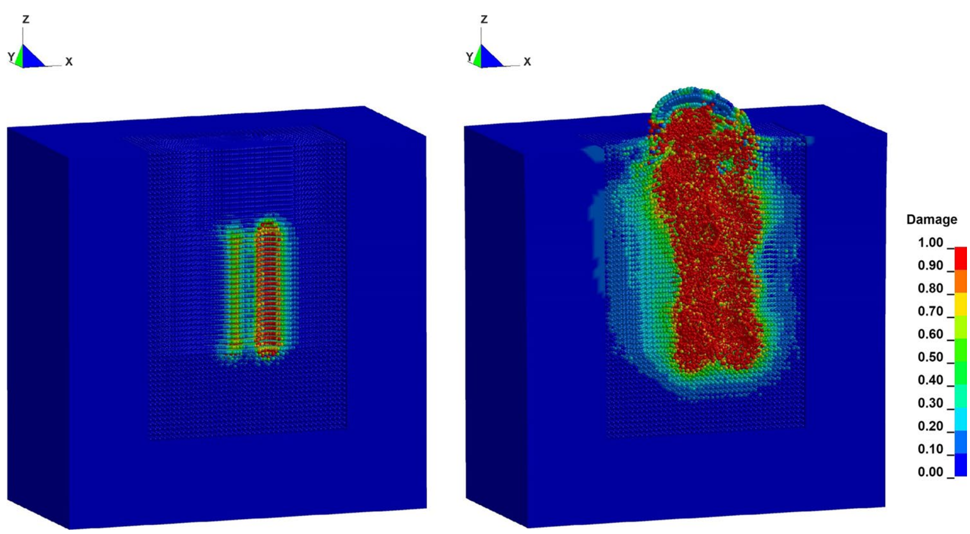

(a) 0.39 ms (b) 11.80 ms

Fig. 12 Continuous charge cut blasting process. **a** 0.39 ms; **b** 11.80 ms charge cut blasting caused a larger damage range to the blasthole's bottom area, and the rock displacement thrown out of the free surface was smaller. This is mainly attributed to the fact that the minimum resistance line of deep hole continuous charge is much higher than that of shallow hole blasting, which makes it difficult for the rock to be thrown out of the free surface. The explosive's energy is more distributed along the radial direction, and the upper rock mass is squeezed out of the free surface, rather than thrown out by the explosion. This results in less damage to the uppermost rock mass and a more concentrated distribution of rock particles thrown out of the free surface.

Figure 13 shows a comparison of the dispersive charge and dispersive charge cut blasting processes. In Fig. 13a, only the upper charge of the dispersive charge is detonated, while all the explosives of the continuous charge are detonated. However, the displacement of the rock thrown out of the free surface by the dispersed charge is significantly larger than that of the continuous charge. The damage of the free surface's outermost rock thrown in the scattered charge mode is between 0.4 and 0.6, while the damage of the outermost rock of the continuous charge is between 0 and 0.2. When *t* is equal to 20.00 ms (Fig. 13b), the particle displacement of the dispersive charge blasting and throwing further increases, and the particle distribution is more dispersed. Moreover, the particle displacement increased by the continuous charge throwing is small, and the particle distribution is concentrated.

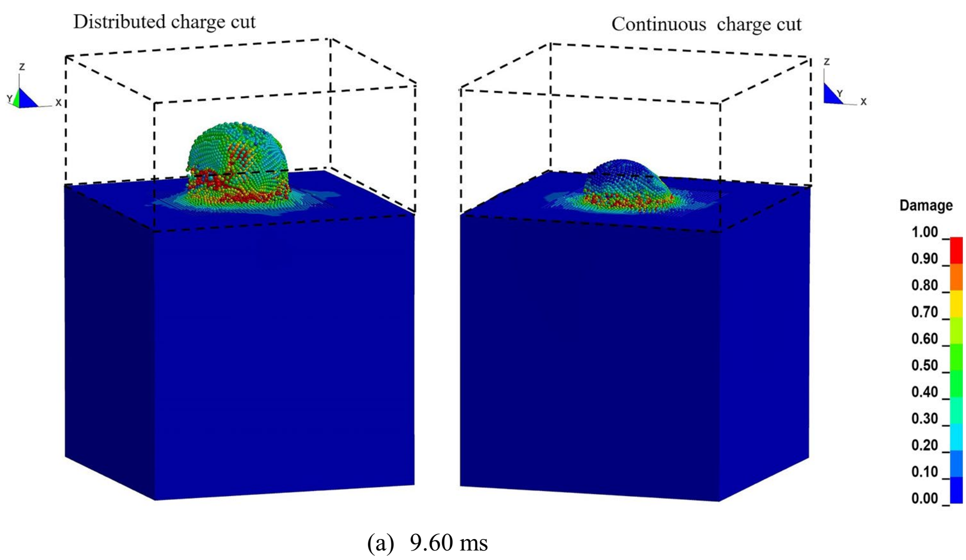

Fig. 13 Comparison of cut blasting process of two charging modes. **a** 9.60 ms; **b** 20.00 ms

The number of rock particles thrown above the free surface is counted (within the black virtual frame). It was noticed that when $t=9.6$ ms, the number of rock particles thrown from the free surface by dispersed charge cut blasting is $N=6293$, and the number of rock particles thrown by continuous charge blasting is $N=6681$. When $t=20$ ms, the number of particles thrown by the dispersed charge and the continuous charge is 13,378 and 10,243, respectively. The number of particles produced by the continuous charge in the blasting's early stage is greater than that of the dispersed charge, but the damage degree of the thrown particles and the displacement of the particles are smaller than those of the dispersed charge. As the blasting progresses, the number of particles thrown by the continuous charge is smaller than that of the dispersed charge, the displacement of the particles thrown by the continuous charge does not increase significantly, and the damage state of the particles in the uppermost layer does not change. By analyzing the number of rock particles thrown out of the free surface and the degree of damage, it can be observed that the dispersed charge is more conducive to the throwing and crushing of rock in deep-hole cutting blasting.

To more intuitively compare the difference in cutting effect under different cutting modes, the cutting efficiency E_c is introduced based on the above particle count statistics. Its meaning is the ratio of the number of rock particles on the free surface to the total number of rock particles within the cutting hole, which is expressed as:

$$E_c = \frac{N}{S_c h / V_p} \tag{29}$$

where S_c is the area of the cut hole area, and V_p is the size of a single SPH particle.

Figure 14 shows the time-varying curve of cut blasting efficiency for continuous charge and dispersed charge. The cut blasting efficiency of continuous charge is only higher than that of dispersed charge over a short period of time, the final cutting efficiency is 64.21%, and the increasing speed of the continuous charge's cutting efficiency decreases significantly in the later stage of blasting. The simulation value of the cutting efficiency of dispersed charge is 83.86%, which is slightly higher than the theoretical value. The cutting efficiency of dispersed charge is about 20% higher than that of continuous charge. The figure also shows a group of deep hole parallel hole cut blasting efficiency obtained from the model test conducted by Zuo et al. and the traditional deep hole cut blasting efficiency obtained from the simulation conducted by Zhang et al. (Zuo et al. 2018; Zhang et al. 2021). The two cases of cut blasting and the arrangement of blast holes for this cut blasting are shown in Fig. 15. The three blasting cases have the same: deep hole, parallel cut holes, center hole, and continuous charge. The difference is the arrangement and number of cut holes. It can be seen that the three cases have high similarities, but the cutting efficiency is about 60%. It is proven that for deep hole cut

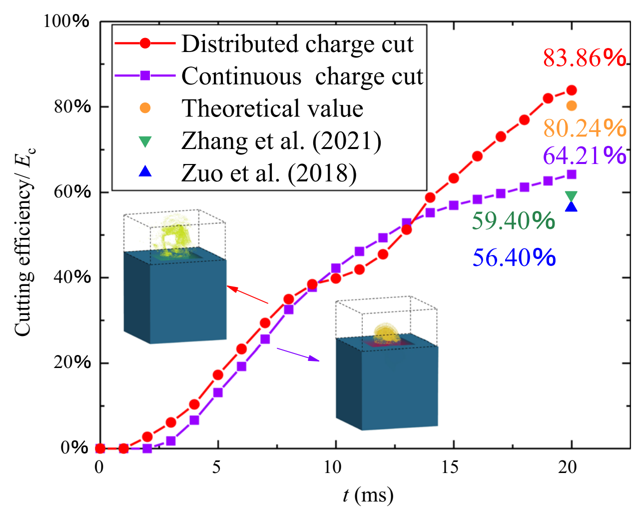

Fig. 14 Comparison of cut blasting efficiency under two charging modes

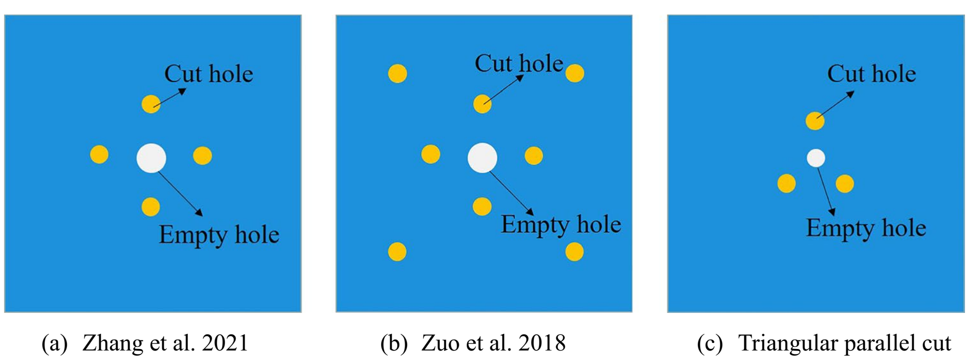

Fig. 15 Several different deep hole cut blasting schemes. **a** Zhang et al. 2021; **b** Zuo et al. 2018; **c** Triangular parallel cut

blasting, the cutting efficiency of continuous charge is low, and changing the arrangement of cutting holes cannot effectively increase the cutting efficiency. However, after using dispersed charge in this paper, the cutting efficiency has been greatly improved, which shows that for deep hole cut blasting, the charge structure has a greater impact on the cutting efficiency.

4 Influence of cutting parameters on blasting effect

In light of the preceding analysis, it can be seen that the use of dispersed charge can improve the cutting efficiency, however, in engineering practice, the parameters affecting the cutting effect are many and complex. Hence, it is necessary to study the influence of various cutting parameters on the cutting efficiency in the case of dispersed charging. This section focuses on the distance between the cutting holes (L), the depth of the cutting holes (h), and the proportion of charge subsections (η) in order to establish the corresponding research model.

4.1 Cut hole spacing

Based on the simulated 450 mm spacing of the cut holes in Sect. 3, models with 350 mm and 550 mm distances are created. Figure 16 shows the cut blasting results for three different cut hole spacings. The three models continue to use the dispersed charge, and all other parameters are the same as in Sect. 3 except for the change in the spacing of the cutting holes. Comparing the blasting results to different hole distances, the particles thrown out of the free surface are relatively dispersed after using the dispersed charge. When $L = 350$ mm, the damage degree of the thrown particles is the highest, and as the hole distance increases, the number of the outermost particles with a low degree of damage increases. When $L = 550$ mm, the damage degree caused by particles thrown from a free surface is greater than that of continuous charge. The displacements of the thrown particles under the three L are similar, and as the hole distance rises, the number of particles thrown out from the free surface increases. It shows that an appropriate extension in the hole spacing based on theoretical calculations can increase the cutting range and the amount of rock thrown. Although too small cutting hole spacing can produce a good cutting effect, it wastes explosive energy and causes excessive rock fragmentation.

4.2 Cut hole depth

The model shown in Fig. 17 changed the depth of the cut hole, while maintaining all other parameters. In engineering practice, the drilling depth impacts the cutting efficiency, and the depth of cutting holes in rock roadway construction is generally about 2.0 m. Deeper drilling results in more pronounced rock entrapment at the bottom of the hole, which decreases the cutting efficiency. Therefore, exploring whether the dispersed charge can solve the low cutting efficiency caused by the increase in hole depth is necessary. The simulation results showed that when the depth of the cut hole is increased by 0.3 m (Fig. 17b) and 0.6 m (Fig. 17c), the rock can be ejected from the cavity's free surface. The degree of damage to rock particles above the free surface

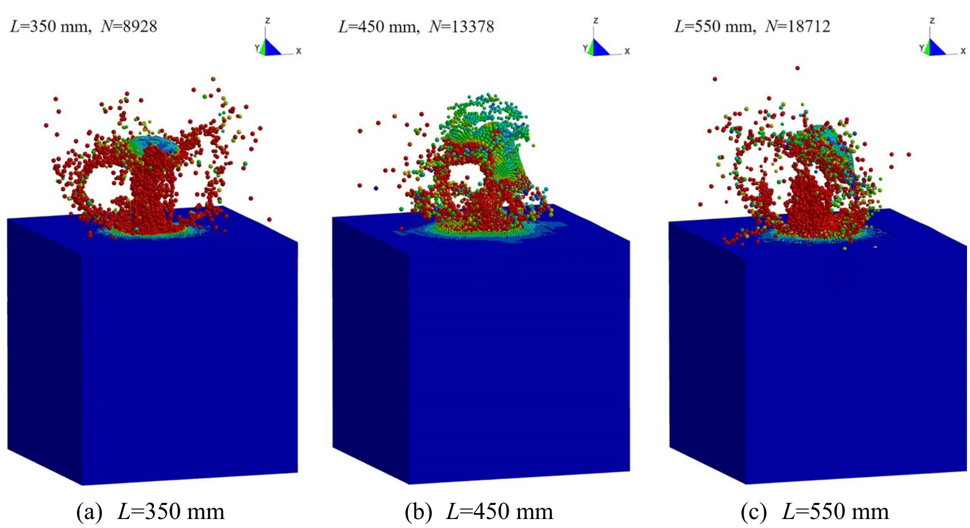

Fig. 16 Different cutting hole spacing. **a** $L = 350$ mm; **b** $L = 450$ mm; **c** $L = 550$ mm

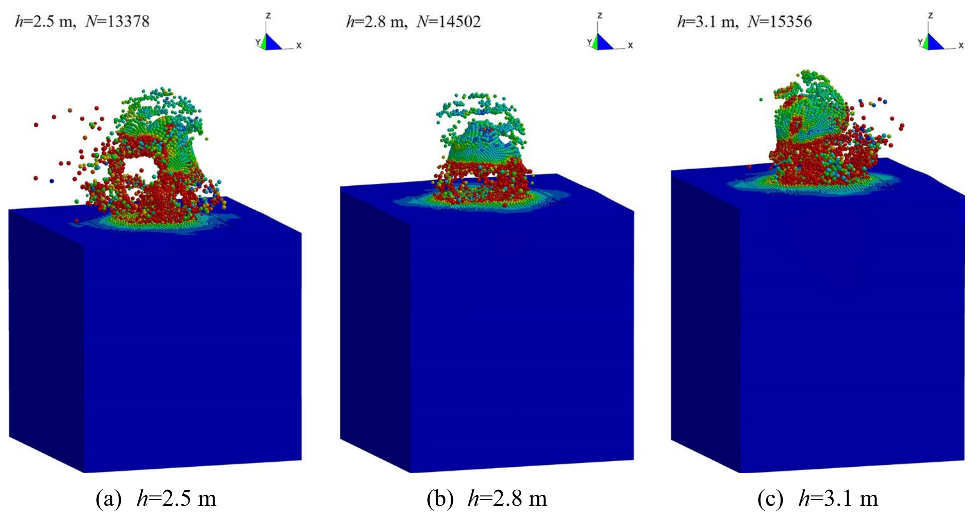

Fig. 17 Different cut hole depths. **a** $h=2.5$ m; **b** $h=2.8$ m; **c** $h=3.1$ m

is comparable across all three model groups, and there is no situation that the outermost rock is not damaged during continuous charging. However, as the hole depth increases, the stratification of rocks with different damage degrees becomes more apparent. It is proved that the dispersed charge can be applied to the cut hole depth in the simulation and can effectively break and throw the rock. The specific effect of hole depth variation on cutting efficiency is further described in Sect. 4.4.

4.3 The proportion of charge in the upper stage

Figure 18 shows the effect of changes in the proportion of upper charge on the cut effect. This section simulates three cases where the upper charge proportions are 0.3, 0.5, and 0.7, respectively. When $\eta=0.3$ (Fig. 18a), the charge in the upper section is low, and the corresponding blocking length and resistance line are smaller. Therefore, the rock can be easily thrown out of the free surface, and the displacement of the rock thrown out of the free surface is the largest. However, due to the excessive charge in the lower section, more explosives are concentrated in the lower part, so that the number of particles finally thrown out of the free surface is the least. When $\eta=0.5$ (Fig. 18b), the particle displacement is in a medium state, and the number of particles thrown out of the free surface is the largest. When $\eta=0.7$ (Fig. 18c), the upper part of the charge has more charges, and the resistance line of the upper rock is also the highest among the three

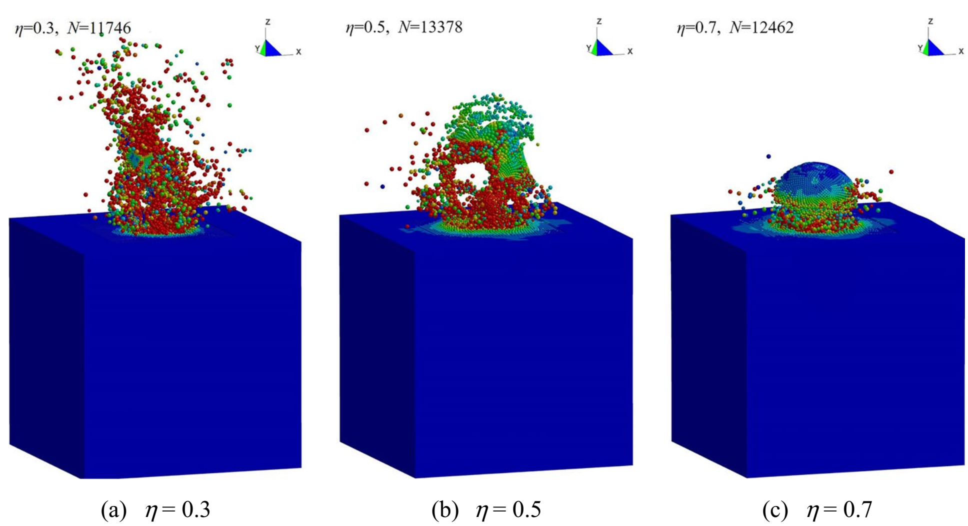

Fig. 18 The proportion of different upper stage charges. **a** $\eta=0.3$; **b** $\eta=0.5$; **c** $\eta=0.7$

models, which makes it difficult to throw the rock corresponding to the upper part of the charge out of the free surface. Although the number of free-surface particles thrown at $\eta = 0.7$ is more than that of $\eta = 0.3$, many particles above the free-surface are not damaged, which is similar to the damage result caused by continuous charging.

Through the analysis, it can be found that the proportion of charge in the upper section obviously influences rock breaking and throwing. However, the number of particles thrown out of the three cut types after using the dispersed charge is more than that of the continuous charge, which proves that the dispersed charge has a promoting effect on the blasting efficiency of deep-hole undercutting.

4.4 Comparison of cutting efficiency

Since the change of the cut hole's depth and distance affect the quantity of rock in the cut area, the factors affect the number of particles thrown out from the free surface. Therefore, it is necessary to use the cutting efficiency as an evaluation index to eliminate the variation in the number of particles caused by the parameters. Figure 19 shows the cutting efficiency of the models corresponding to different cutting parameters. Figure 19a reveals that the cutting efficiency decreases as the cutting hole spacing increases. In practical engineering applications, the cutting hole spacing must be adjusted based on the rock fragmentation degree and the consumption of explosives. Figure 19b shows that the cutting efficiency decreases as the cut hole depth increases. The clamping effect at the bottom of the blast hole becomes more evident with the increase of hole depth, making it more difficult to throw the rock mass at the lower part. It is worth noting that although increasing the depth of the hole reduces the cutting efficiency, the blasting cutting efficiency of the deepest cutting hole ($h = 3.1$ m) with dispersed charge is still significantly higher than that of continuous charge. Therefore, cutting efficiency can be improved during construction by raising the unit consumption of explosives in the lower section. Figure 19c shows that the upper section's charge ratio also impacts the cutting efficiency. The cutting effect will be poor when the value is large or small. Under the simulation conditions described in this paper, the cutting efficiency of $\eta = 0.5$ is the highest, and the cutting efficiency corresponding to three different η values is higher than that of continuous charging.

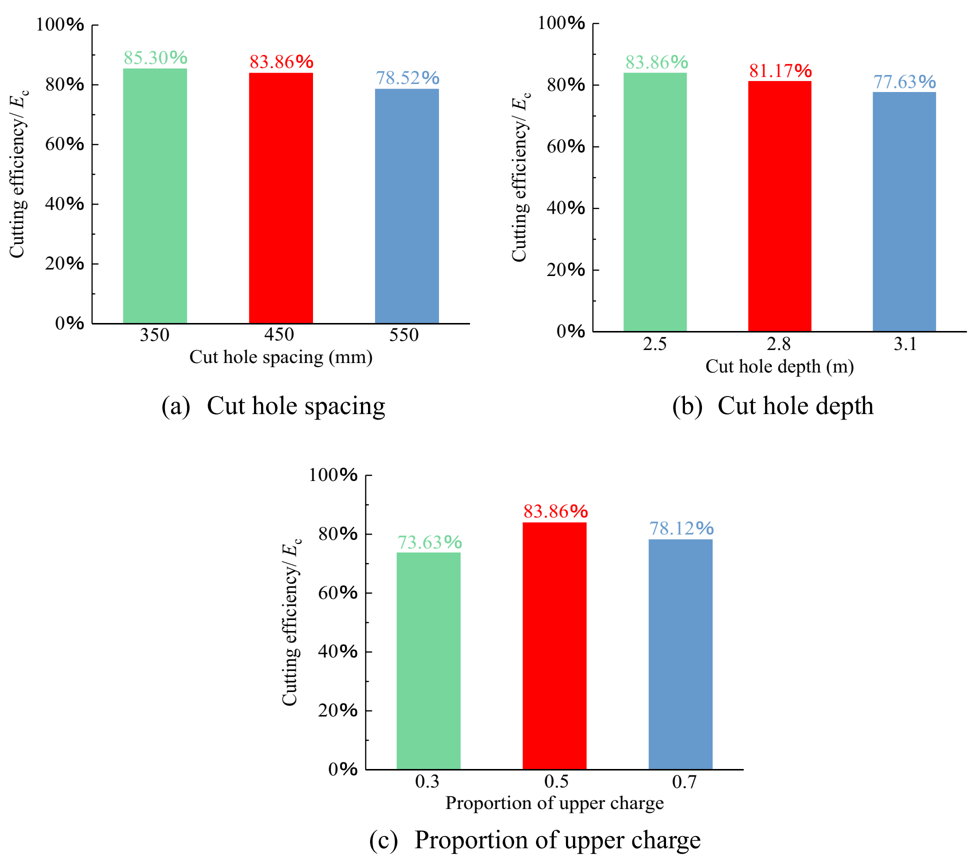

Fig. 19 Cutting efficiency corresponding to different cutting parameters. **a** Cut hole spacing; **b** Cut hole depth; **c** Proportion of upper charge

5 Engineering practice

5.1 Engineering overview

Gubei Coal Mine is located in Fengtai County, Huainan City, Anhui Province, China. The test roadway is the belt conveyor crosscut of the north-1 coal panel. The working section is a 4.4 m × 5.6 m semi-circular arch with a straight wall, and the tunnelling method is drilling and blasting. The roadway's lithology consists primarily of grey sandstone.

5.2 Engineering case

In the previous construction design for the above-mentioned experimental tunnel, continuous charging was adopted, the depth of the cut hole was between 1.8 m and 2.0 m, and the blasthole utilization rate was 70% to 85%. The borehole diameter was 42 mm. The explosives are three-level water gel explosives. When the borehole is shallow, the above blasting design can achieve a good effect and meet production requirements. However, the increasing demand for coal and the need to reduce the number of operations make shallow hole excavation and blasting obsolete. In light of the preceding context, the experimental roadway conducted deep hole cutting blasting to increase the single excavation depth. However, the traditional continuous charge is unsuitable for deep hole cut blasting. In conjunction with the research results of numerical simulation, it has been decided to use the combination of dispersed charge and digital electronic detonator for the deep hole cut blasting.

Figure 20 shows the blasting diagram of on-site blasting practice. The double triangle method is applied to arrange the cut holes in the construction due to the large cross-sectional area (Fig. 20a). The distance between each hole is 650 mm. The depth of all cutting holes is 2.8 m, and the cutting blasting is carried out using the dispersed charge technology. Other holes have a depth of 2.4 m. Figure 20b shows the charge structure and detonation sequence of the cut hole. When loading explosives, the upper charge ratio is controlled to be 0.5. Two digital electronic detonators are placed in each cutting hole, and the detonation sequence is as follows: The upper section of the first-stage undercut is detonated, the lower section of the first-stage undercut is detonated, the upper section

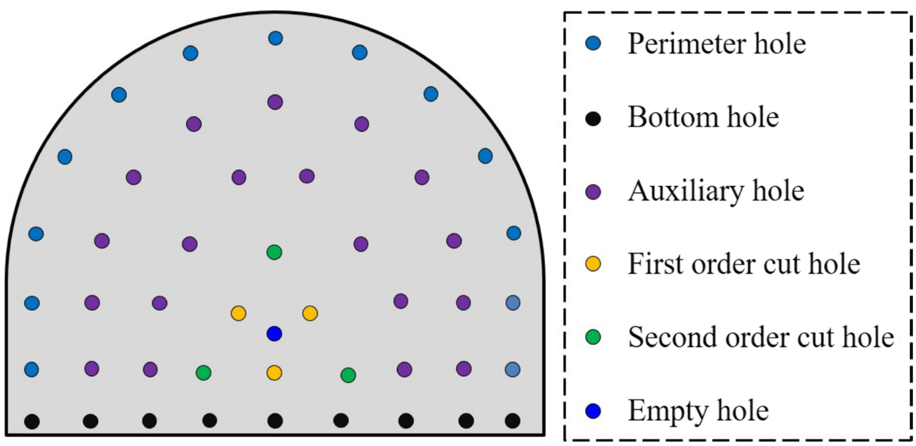

(a) Hole layout of the blasting workface

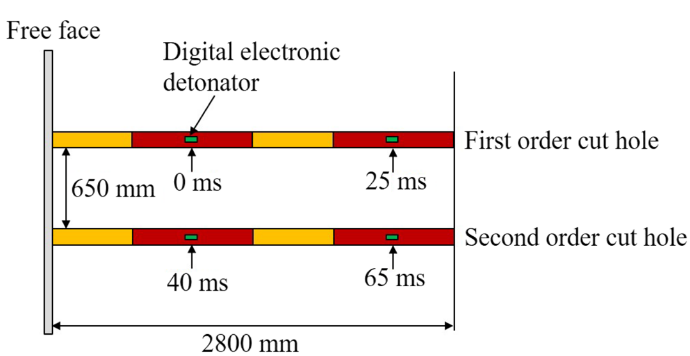

(b) Charge structure of cut hole

Fig. 20 Blasting design drawing. **a** Hole layout of the blasting workface; **b** Charge structure of cut hole of the second-stage undercut is detonated, and the lower section of the second-stage undercut is detonated. The blasting sequence of other blasting holes is the same as that of traditional blasting.

According to the specific conditions of the above engineering cases, we established a double-triangular undercut blasting model. The size of the model is 4 m×6 m×4.8 m, the cutting hole parameters are the same as in Fig. 20, and the material parameters are the same as those in Sect. 3.3.2. Considering that the long delay time will affect the calculation time and difficulty, the inter-well delay and the intra-well delay in the simulation are both 10 ms. Figure 21 shows the double triangular cut blasting process. Figure 21a shows the rock throwing results when the first-order undercuts are blasted, and Fig. 21b shows the rock throwing effects when the second-order undercuts are blasted. The simulation results show that adding a circle of undercut holes to the model in Sect. 3.3 can increase the area of the undercut area, thereby increasing the volume of the cavity created by the undercut holes. The detonation of the first-order undercuts provides more free surfaces for the detonation of the second-order undercuts, which makes the detonation of the second-order undercuts easier. However, due to the increased hole spacing, the number of rock particles with less damage increased.

Figure 22 shows the use of the electronic detonator and the blasting result. In Fig. 22a, the using and connection of the digital electronic detonator is performed according to the blasting design. After employing the digital electronic detonator, the connection time is greatly decreased, and the inspection efficiency of the detonation network is improved. Figure 22b represents the photo of roadway roof after blasting. The half hole marks are clearly visible in the image, proving that the cutting effect is satisfactory, and the subsequent peripheral holes also achieve a good blasting effect. Figure 22c depicts a front view of the cross-section, which is smooth to reduce the subsequent cleaning of suspended gravel and support time. After the explosion, gravel distribution was reasonable, and no large pieces stood out. After many tests, the single excavation depth of the blasting section of the roadway is 2.2–2.3 m, and the depth of the cutting area is 2.6–2.8 m. The average blasthole utilization rate is above 90%, the section excavation depth is increased from 70 to 100 m every month, and the roadway excavation speed is increased by 40%. The field test results show that the use of dispersive charge and digital electronic detonator delay initiation can greatly improve the cutting efficiency and driving efficiency.

6 Conclusions

This paper introduces a dispersed charge cut blasting method suitable for the deep hole cut blasting. The cut blasting mechanism of dispersed charge is introduced

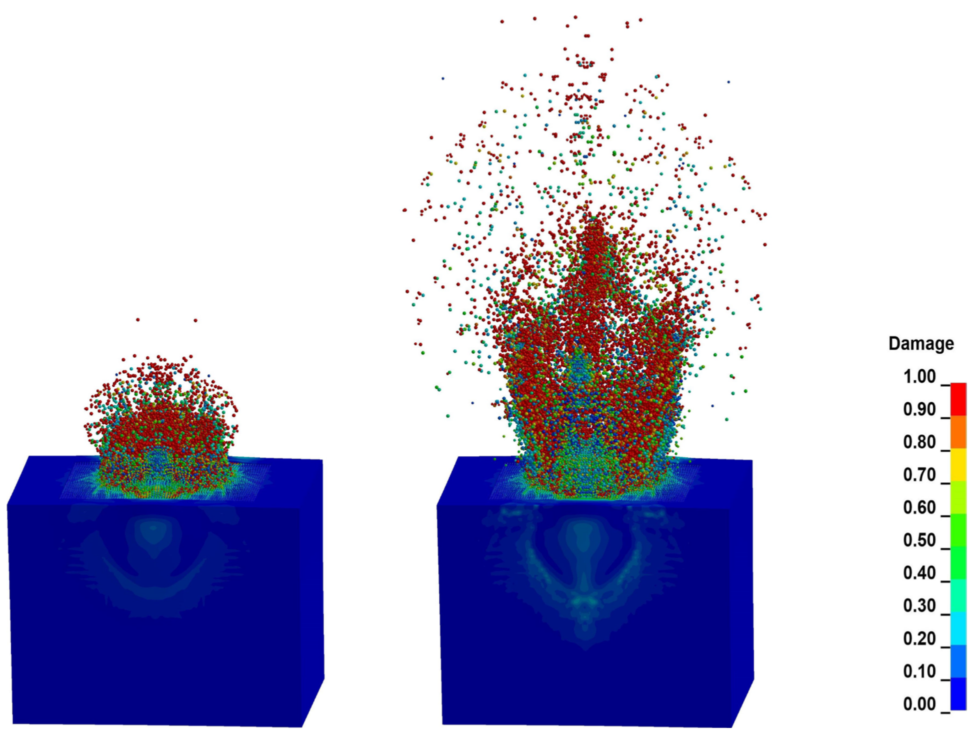

(a) First order cut hole blasting (b) Second order cut hole blasting

Fig. 21 Double triangle cut blasting. **a** First order cut hole blasting; **b** Second order cut hole blasting

(a) The use of electronic detonators

(b) Half hole mark of section profile

(c) Section after blasting

Fig. 22 Drilling and blasting process of on-site working face. **a** Setting time of digital electronic detonator; **b** Half hole mark of section profile; **c** Section after blasting

through the theoretical model, the cutting parameters are theoretically determined, and the cutting efficiency is defined. A deep-hole cut blasting model of dispersed charge and the continuous charge is built using the SPH-FEM method, and the cut blasting process and the change of cutting efficiency under the two charge modes are compared. The influence of several critical cutting parameters is investigated based on determining that the dispersed charge is beneficial for improving of cutting efficiency. The research results are integrated with digital electronic detonators and successfully implemented in engineering practice. The following findings are:

(1) During the early stage of deep hole cut blasting, the continuous charge throws more rock particles, but the number of particles thrown out at the end is much smaller than that of the dispersed charge. The continuous charge causes the explosive to have more effect on the rock mass at the bottom of the blasthole, and less on the thrown particles. The use of continuous charge

in deep holes cannot significantly increase the cutting efficiency by adjusting the hole arrangement.

(2) The dispersed charge hurls the upper rock mass by reducing the resistance line and creating a new free surface for the lower rock mass blasting. The cutting efficiency of dispersed charge is higher than that of continuous charge, and its maximum cutting efficiency is about 20% greater than that of continuous charge, and the particle damage and displacement are also larger than those of continuous charge.

(3) Increasing the spacing and depth of the cut holes decreases the cutting efficiency. The charge proportion in the upper section significantly impacts the cutting efficiency and the change of rock damage. When the charge proportion in the upper section is 0.5, the cutting efficiency reaches its highest, consistent with the calculated theoretical value.

(4) The field engineering application results showed that the dispersive charge integrated with the digital electronic detonator is applied to the deep hole excavation blasting, improving the rock breakage and excavation efficiency.

Acknowledgements This work is financed by the State Key Development Program for Basic Research of China (2016YFC0600903) and the National Natural Science Foundation of China (51934001).

Declarations

Competing interests The authors declare that they have no conflicts of interest to this work.

References

Adhikari GR, Babu AR, Balachander R, Gupta RN (1999) On the application of rock mass quality for blasting in large underground chambers. Tunn Undergr Space Technol 14(3):367–375

Alia A, Souli M (2006) High explosive simulation using multi-material formulations. Appl Therm Eng 26(10):1032–1042

Amiri HS, Murthy VM (2019) Optimising blast pulls and controlling blast-induced excavation damage zone in tunnelling through varied rock classes. Tunn Undergr Space Technol 85:307–318

Cheng B, Wang HB, Zong Q, Xu Y, Wang MX, Zhu NN (2021) Study on the novel technique of straight hole cutting blasting with a bottom charged central hole exploded supplementally. Arab J Geosci 14:2867–2878

Dai J, Yang YQ (2000) Researches on blasting parameters of triangle burn cut. Explos Shock Waves 20(4):364–368

Ding CX, Yang RS, Zheng CD, Yang LY, He SL, Feng C (2021) Numerical analysis of deep hole multi-stage cut blasting of vertical shaft using a continuum-based discrete element method. Arab J Geosci 14:1086–1096

Esmaeili M, Tavakoli B (2019) Finite element method simulation of explosive compaction in saturated loose sandy soils. Soil Dyn Earthq Eng 116:446–459

Gong M, Wang CH, Liang LX, Wang H, Wen B, Wu HJ (2015) Function analysis and confirming method of key blasting parameters for excavating in hard rock. J China Coal Soc 40(7):1526–1533

Henrych J (1979) The dynamics of explosion and its use. Elsevier, Amsterdam, pp 358–372, 412–457

Himanshu VK, Mishra AK, Roy MP, Vishwakarma AK, Singh PK (2021) Numerical simulation based approach for assessment of blast induced deformation pattern in slot raise excavation. Int J Rock Mech Min Sci 144:104816

Jayasinghe LB, Shang JL, Zhao ZY, Goh ATC (2019) Numerical investigation into the blasting-induced damage characteristics of rocks considering the role of in-situ stresses and discontinuity persistence. Comput Geotech 116:103207

Johnson GR, Holmquist TJ (2011) A computational constitutive model for glass subjected to large strains, high strain rates and high pressures. J Appl Mech Trans ASME 78(5):051003

Li HT (2016) The study of the rock RHT model and to determine the values of main parameters. China University of Mining and Technology

Li Q, Zhang SX, Wang MH, Guo Y, Xu WL, Feng DD (2019) Study on the influence of length-diameter ratio on the mechanical characteristics of cracks at the end of linear charges. J Min Sci Technol 4(2):112–119

Li MZ, Ma ZM, Xue DL, Yuan YH (2020) Research of cumulative energy blasting technology with deep and shallow hole combined in hard roof. J Min Sci Technol 5(6):616–623

Li SL, Liang SF, Li C, Liu DS (2021) Current status and development trend of deep hole bench blasting technology in open-pit mines. J Min Sci Technol 6(5):598–605

Li YL, Yang RS, Fang SZ, Lin H, Lu SJ, Zhu Y, Wang MS (2022) Failure analysis and control measures of deep roadway with composite roof: a case study. Int J Coal Sci Technol 9(1):2. https://doi.org/10.1007/s40789-022-00469-1

Lin CM, Chen SH (1997) Study on the fragment discharge process in deep hole parallel-cut blasting. Explos Shock Waves 17(1):69–70

Lin DN, Chen SR (2005) Theoretical and testing study on factors affecting parallel hole cut blasting. J China Coal Soc 30(1):40–43

Liu K, Li QY, Wu CQ, Li XB, Li J (2018) A study of cut blasting for one-step raise excavation based on numerical simulation and field blast tests. Int J Rock Mech Min Sci 109:91–104

Liu F, Chang KL, Li M (2019) Numerical simulation on the influence of boreholes arrangement and delay time on coal crushing effects. J Min Sci Technol 4(4):318–326

Liu XY, Gong M, Wu JH, An D (2021) Determination method of tunnel blasting parameters using electronic detonator under changing condition of free surface. Explos Shock Waves 41(10):153–165

Lu WB, Yang JH, Yan P, Chen M, Zhou CB, Luo Y, Jin L (2012) Dynamic response of rock mass induced by the transient release of in-situ stress. J Rock Mech Min Sci 53:129–141

Qiu XY, Shi XZ, Gou YG, Zhou J, Chen J, Chen H, Huo XF (2018) Short-delay blasting with single free surface: results of experimental tests. Tunn Undergr Space Technol 74:119–130

Saadatmand HA, Katsabanis P (2020) The effect of stress wave interaction and delay timing on blast-induced rock damage and fragmentation. Rock Mech Rock Eng 53:2327–2346
Shapiro VY (1989) Efficiency of cut configuration in driving tunnels with a set of deep blast holes. J Min Sci 25(4):379–386
Soroush K, Mehdi Y, Arash E (2015) Trend analysis and comparison of basic parameters for tunnel blast design models. Int J Min Sci Technol 25(4):595–599
Tang JP, Zhang X, Sun SJ, Pan YS, Li LP (2022) Evolution characteristics of precursor information of coal and gas outburst in deep rock cross-cut coal uncovering. Int J Coal Sci Technol 9(1):5. https://doi.org/10.1007/s40789-022-00471-7
Wang WG, Chen YM, Liu HL, Zhang ZC (2013) Numerical simulation of explosion in soil based on a coupled SPH-FEM algorithm. Rock Soil Mech 34(7):2104–2110
Wang HB, Xu X, Zong Q, Xu SM, Xu Y (2017) Research and application of hard rock deep-hole advance blasting in comprehensive roadway excavation. J China Coal Soc 42(4):908–915
Wang ZL, Wang HC, Wang JG, Tian NC (2021) Finite element analyses of constitutive models performance in the simulation of blast-induced rock cracks. Comput Geotech 135:104172
Xie LX, Lu WB, Zhang QB, Jiang QH, Wang GH, Zhao J (2016a) Damage evolution mechanisms of rock in deep tunnels induced by cut blasting. Tunn Undergr Space Technol 58:257–270
Xie LX, Lu WB, Zhang QB, Jiang QH, Wang GH, Zhao J (2016b) Damage evolution mechanisms of rock in deep tunnels induced by cut blasting. Tunn Undergr Space Technol Space Technol 58:257–270
Yang RS, Zhang ZR, An C, Zhen CD, Ding CX, Xiao CL (2020) Discussion on ultra-deep depth problem of slot hole in blasting excavation of rock roadway in coal mine. Coal Sci Technol 48(1):10–23
Yue ZW, Yang RS, Guo DM, Niu XC, Ma XM (2009) Model experimental of stress field around empty hole under blasting loading. J China Coal Soc 34(5):624–628
Zhang Q, Yang YQ, Wang SR, Wang ZQ (2000) Formation and function of blasting funnel at cut cavity. Eng Blast 6(1):21–24
Zhang ZR, Chen HY, Jiao WG, Yu TF (2020) Rock breaking mechanism and blasting parameters of straight hole cutting with empty-hole. J China Coal Soc 45(2):791–800
Zhang H, Li TC, Wu S, Zhang XT, Gao W, Shi QP (2022) A study of innovative cut blasting for rock roadway excavation based on numerical simulation and field tests. Tunn Undergr Space Technol 119:104233
Zong Q (1997) Investigation on features of rock quasi-static fragmentation by gaseous explosion product. Rock Soli Mech 18(2):73–78
Zuo JJ, Yang RS, Xiao CL, Lei JL, Zhao Y (2018) Model test of empty hole cut blasting in coal mine rock drivage. J Min Sci Technol 3(4):335–341